Physics Letters B 677 (2009) 16–23

Contents lists available at ScienceDirect

Physics Letters B

www.elsevier.com/locate/physletb

Detecting relic gravitational waves in the CMB: Comparison of Planck and ground-based experiments

Wen Zhao [a,b,c,*], Wei Zhang [d]

[a] School of Physics and Astronomy, Cardiff University, Cardiff, CF24 3AA, United Kingdom
[b] Wales Institute of Mathematical and Computational Sciences, Swansea, SA2 8PP, United Kingdom
[c] Department of Physics, Zhejiang University of Technology, Hangzhou, 310014, People's Republic of China
[d] National Astronomical Observatories, Chinese Academy of Sciences, Beijing, 100012, People's Republic of China

ARTICLE INFO

Article history:
Received 20 March 2009
Received in revised form 6 May 2009
Accepted 8 May 2009
Available online 13 May 2009
Editor: T. Yanagida

PACS:
98.70.Vc
98.80.Cq
04.30.-w

ABSTRACT

We compare the detection abilities for the relic gravitational waves by two kinds of forthcoming cosmic microwave background radiation (CMB) experiments, space-based Planck satellite and the various ground-based experiments. Comparing with the ground-based experiments, Planck satellite can observe all the CMB power spectra in all the multipole range, but having much larger instrumental noises. We find that, for the uncertainty of the tensor-to-scalar ratio Δr, PolarBear (II) as a typical ground-based experiment can give much smaller value than Planck satellite. However, for the uncertainty of the spectral index Δn_t, Planck can give the similar result with PolarBear (II). If combining these two experiments, the value of Δn_t can be reduced by a factor 2. For the model with $r = 0.1$, the constraint $\Delta n_t = 0.10$ is expected to be achieved, which provides an excellent opportunity to study the physics in the inflationary universe. We also find the observation in the largest scale ($\ell < 20$) is very important for constraining the spectral index n_t. So it is necessary to combine the observations of the future space-based and ground-based CMB experiments to determine the relic gravitational waves.

1. Introduction

Relic gravitational waves (RGWs) are generated in the very early Universe due to the superadiabatic amplification of zero point quantum fluctuations of the gravitational field [1,2], and freely evolve in the whole stage of the Universe [3,4]. So RGWs carry invaluable information about early history of our Universe inaccessible to any other medium.

Detection of RGWs is rightly considered a highest priority for the upcoming cosmic microwave background radiation (CMB) experiments. The current CMB experiments are yet to detect a definite signature of RGWs [5]. In the near future, the successive generation of the experiments, including the space-based Planck satellite [6] and the various ground-based experiments [7–10] together with a host of balloon-borne experiments [11] will provide an increasing sensitive measurement of RGWs.

The space-based experiments, as COBE, WMAP and Planck satellites, can remove atmospheric noises and observe the fairly cleaned CMB temperature and polarization anisotropy fields. In addition, the space-based experiments provide the unique opportunity to detect the CMB power spectra in the largest scale ($\ell < 20$) by surveying the full sky.

At the same time, the CMB polarization field can also be observed by the ground-based experiments. Since the atmospheric emission is not expected to be linearly polarized [12], by integrating deeply on the relatively small patches of sky, it is possible to make a measurement of the polarization anisotropies with a comparable signal-to-noise ratio to a satellite experiment on all but the largest angular scales.

In this Letter, we shall investigate the detection abilities for the RGWs, by the observations of the forthcoming generation of the ground-based and space-based experiments. By calculating the constraints on the tensor-to-scalar ratio r and the tensor spectral index n_t, we shall compare the detection abilities of these two types of experiments. We also investigate the potential improvement of the detection ability by combining the observations of them.

2. Review of primordial perturbations, CMB and noises

2.1. Primordial perturbation power spectra

The main contribution to the temperature and polarization anisotropies of the CMB comes from two types of cosmological perturbations, density perturbations (also known as the scalar per-

* Corresponding author at: School of Physics and Astronomy, Cardiff University, Cardiff, CF24 3AA, United Kingdom.
E-mail address: wen.zhao@astro.cf.ac.uk (W. Zhao).

0370-2693/$ – see front matter
doi:10.1016/j.physletb.2009.05.015

turbations) and RGWs (also known as the tensor perturbations). The primordial power spectra of these perturbations are usually assumed to be power laws, which is a generic prediction of a wide range of scenarios of the early Universe [13]. If we ignore the running of the spectral indices, the primordial spectra can be written as the following simple forms

$$P_s(k) = A_s(k_0)(k/k_0)^{n_s-1}, \tag{1}$$

$$P_t(k) = A_t(k_0)(k/k_0)^{n_t}, \tag{2}$$

where k_0 is the pivot wavenumber, which can be arbitrarily chosen. n_s and n_t are the scalar and tensor spectral indices. The tensor-to-scalar ratio is defined by

$$r(k_0) \equiv \frac{A_t(k_0)}{A_s(k_0)}. \tag{3}$$

For a fixed A_s, the primordial power spectra of RGWs are completely determined by two parameters r and n_t, if a power-law form in (2) is assumed. The simplest single-field slow-roll inflationary models predict a consistency relation between r and n_t [13]: $n_t = -r/8$. However, this consistency relation is incorrect for other inflationary models [14]. So the determination the parameters r and n_t by the observations, provides an excellent opportunity to distinguish various inflationary-type models.

Since in this Letter, we are primarily interested in the parameters of the RGW field, in the analysis below we shall work with a fixed cosmological background model. More specifically, we shall work in the framework of ΛCDM model, and keep the background cosmological parameters fixed at the values determined by a typical model [15]

$$h = 0.732, \qquad \Omega_b h^2 = 0.02229,$$
$$\Omega_m h^2 = 0.1277, \qquad \Omega_k = 0, \qquad \tau_{\rm reion} = 0.089. \tag{4}$$

Furthermore, in order to show the results in the figures, we adopt the following parameters of the density perturbations and tensor spectral index,

$$A_s = 2.3 \times 10^{-9}, \qquad n_s = 1, \qquad n_t = 0. \tag{5}$$

2.2. CMB power spectra and their estimators

Let us turn our attention to the CMB field. Density perturbations and gravitational waves produce temperature and polarization anisotropies in the CMB characterized by four angular power spectra C_ℓ^T, C_ℓ^E, C_ℓ^B and C_ℓ^C as functions of the multipole number ℓ [16–19]. Here C_ℓ^T is the power spectrum of the temperature anisotropies, C_ℓ^E and C_ℓ^B are the power spectra of the so-called E-mode and B-mode polarizations and C_ℓ^C is the power spectrum of the temperature-polarization cross correlation.

In the linear theory, the various power spectra C_ℓ^Y (where $Y = T, E, B$ or C) can be presented in the following form

$$C_\ell^Y = C_{\ell,s}^Y + C_{\ell,t}^Y, \tag{6}$$

where $C_{\ell,s}^Y$ are the power spectra due to the density perturbations, and $C_{\ell,t}^Y$ are the power spectra due to RGWs.

The CMB power spectra C_ℓ^Y are theoretical constructions determined by ensemble averages over all possible realizations of the underlying random process. However, in real CMB observations, we only have access to a single sky, and hence to a single realization. In order to obtain information on the power spectra from a single realization, it is required to construct estimators of power spectra D_ℓ^Y [20]. The probability distribution functions for the estimators are detailed described in [20], which predicts the expectation values of the estimators

$$\langle D_\ell^Y \rangle = C_\ell^Y, \tag{7}$$

and the standard deviations [20]

$$(\sigma_{D_\ell^X})^2 = \frac{2(C_\ell^X + N_\ell^X)^2}{(2\ell+1) f_{\rm sky}} \quad (X = T, E, B),$$
$$(\sigma_{D_\ell^C})^2 = \frac{(C_\ell^T + N_\ell^T)(C_\ell^E + N_\ell^E) + (C_\ell^C)^2}{(2\ell+1) f_{\rm sky}}, \tag{8}$$

where $f_{\rm sky}$ is the cut-sky factor, and N_ℓ^X are the noise power spectra, determined by the specific experiments.[1]

2.3. Noise power spectra

Considering an experiment with multiple frequency channels, the total instrumental noise power spectra can be approximately presented as (see for instance [22]),

$$N_\ell^X = \left(\sum_c \frac{1}{N_{\ell,c}^X} \right)^{-1}. \tag{9}$$

Here $N_{\ell,c}^X$ is the noise power spectrum for the individual frequency channel, which is given by

$$N_{\ell,c}^X = \left(\sigma_{\rm pix}^X \cdot \theta_{\rm F}\right)^2 \cdot \exp\left[\ell(\ell+1) \frac{\theta_{\rm F}^2}{8 \ln 2} \right]. \tag{10}$$

In this formula, $\theta_{\rm F}$ is the full width half maximum (FWHM) beam size. The pixel noises $\sigma_{\rm pix}^X$ depend on the survey design and the instrumental parameters.

First, let us focus on the space-based Planck satellite. In this Letter, we consider four frequency channels for the Planck satellite, which are listed in Table 1. After two full sky survey (14 months), the pix noises $\sigma_{\rm pix}^X$ are expected to be the values listed in Table 1 for different channels. In Fig. 1, we plot the instrumental noise power spectrum N_ℓ^B, as a comparison with the values of CMB power spectrum C_ℓ^B in the model with $r = 0.1$ and $r = 0.01$. We find, in the model of $r = 0.1$, the value of C_ℓ^B is larger than that of N_ℓ^B only at the largest scale. So Planck satellite can detect RGWs mainly by the observation in this largest scale, which will be clearly shown in the following section.

For a ground-based experiment with N_d detectors, a solid angle per pixel $\theta_{\rm F}^2$ and a sensitivity NET, we assume it will survey an area $4\pi f_{\rm sky}$ in the integration time $t_{\rm obs}$. The pixel polarization noises are

$$\left(\sigma_{\rm pix}^E\right)^2 = \left(\sigma_{\rm pix}^B\right)^2 = \frac{(\sqrt{2}{\rm NET})^2 \cdot 4\pi f_{\rm sky}}{t_{\rm obs} N_d \theta_{\rm F}^2}. \tag{11}$$

In this Letter, we shall discuss five kinds of ground-based experiments: BICEP, PolarBear (I) and (II), QUIET (I) and (II). The instrumental parameters for these experiments are given in Appendix A. Notice that, the ground-based experiments are only sensitive to the polarizations. Since the ground-based experiments can only survey a small part of the full sky, it cannot encode the information of CMB field in the very large scale. From Fig. 1, we find that ground-based experiments have much smaller noise power spectra than Planck satellite.

We should notice that, cosmic lensing can convert the E-mode polarization into B-mode (see [23] for a review). So the B-mode spectrum due to RGWs will be contaminated by a cosmic lensing contribution. The lensed C_ℓ^B is also shown in Fig. 1, which can be treated as a part of the total noise power spectrum N_ℓ^B as well as instrumental noise power spectra in (9).

[1] For the actual observations of the ground-based experiments, we always have to bin the observed data to keep the data at different ℓ being uncorrelated [21]. However, the bin does not affect our conclusion in this Letter.

Table 1
Instrumental parameters for Planck satellite [6].

Band center [GHz]	100	143	217	353
$\sigma^T_{\rm pix}$ [μK]	6.8	6.0	13.1	40.1
$\sigma^E_{\rm pix}$ and $\sigma^B_{\rm pix}$ [μK]	10.9	11.5	26.8	81.4
FWHM [arcmin]	9.5	7.1	5.0	5.0
$f_{\rm sky}$	0.65			
ℓ range	2–1000			
Integration time	14 Months			

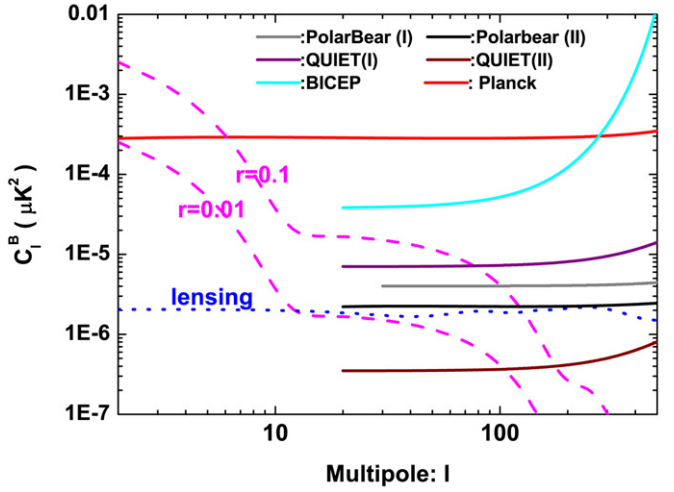

Fig. 1. This figure shows the instrumental noise power spectrum N^B_ℓ for Planck satellite and various ground-based experiments (solid lines). For the comparison, we also plot the power spectra C^B_ℓ in the models with $r = 0.1$ and $r = 0.01$ (magenta dashed lines). The blue dotted line denotes the power spectra C^B_ℓ generated by cosmic lensing. (For interpretation of the references to colour in this figure legend, the reader is referred to the web version of this Letter.)

In addition to the instrumental noises and lensing noise, various foregrounds, such as the synchrotron and dust, are also the important contaminations in the CMB observation. It is hoped that the multifrequency observations and the hard work by astronomical community might allow future experiments can reduce the foreground noises in a very accurate level (see for instance [24]). So in the following discussion, we shall not consider this kind of contamination.

3. Determination of RGWs by CMB observations

In the previous works [20,25,26], we have discussed how to best constrain the parameters of the RGWs, i.e. r and n_t, by the CMB observation. In the paper [26], we found that, in general the constraints on r and n_t correlate with each other. However, if we consider the tensor-to-scalar ratio at the best-pivot wavenumber k^*_t, i.e. $r \equiv r(k^*_t)$, the constraints on r and n_t becomes independent of each other, and the uncertainties Δr and Δn_t have the minimum values. In the work [26], we have derived the formulas to calculate the quantities: the best-pivot wavenumber k^*_t, and the uncertainties of the parameters Δr and Δn_t. This provides a simple and quick method to investigate the ability of the CMB observations for the detect of RGWs. In this section, we shall briefly introduce these results.

It is convenient to define two quantities as below,

$$a^Y_\ell \equiv \frac{C^Y_{\ell,t}}{\sigma_{D^Y_\ell}}, \qquad b^*_\ell \equiv \ln\left(\frac{\ell}{\ell^*_t}\right). \tag{12}$$

Here $C^Y_{\ell,t}$ are the CMB power spectra generated by RGWs, and $\sigma_{D^Y_\ell}$ are the standard deviations of the estimators D^Y_ℓ, which can be calculated by Eq. (8). ℓ^*_t is the best-pivot multipole, which is determined by solving the following equation [26]:

$$\sum_\ell \sum_Y a^{Y2}_\ell b^*_\ell = 0. \tag{13}$$

So the value of ℓ^*_t depends on the cosmological model, the amplitude of RGWs, and the noise power spectra. The best-pivot wavenumber k^*_t relates to ℓ^*_t by the approximation [26],

$$k^*_t \simeq \ell^*_t \times 10^{-4}\ {\rm Mpc}^{-1}. \tag{14}$$

In order to determine the constraints on the RGWs from the CMB observation, we can consider two quantities, the signal-to-noise ratio S/N (which directly relate to Δr) and uncertainty Δn_t. For a specific cosmological model and the noises, these quantities can be calculated by the following formulas [20,25,26]

$$S/N \equiv r/\Delta r = \sqrt{\sum_\ell \sum_Y a^{Y2}_\ell},$$
$$\Delta n_t = 1/\sqrt{\sum_\ell \sum_Y \left(a^Y_\ell b^*_\ell\right)^2}. \tag{15}$$

In this Letter, in order to compare the detection abilities for RGWs of Planck and the ground-based experiments, we shall consider the following four cases:

Case A: We only consider the observation of the B-polarization by Planck satellite. So, in Eqs. (13) and (15), $Y = B$ and $\ell = 2$–1000. The noise power spectrum N^B_ℓ and cut sky factor $f_{\rm sky}$ are the corresponding quantities for Planck satellite.

Case B: We only consider the observation of the B-polarization by the ground-based experiments.

Case C: We consider the determination on the RGWs by combining the B-polarization observations of Planck and the various ground-based experiments. Since the power spectra in the scale $\ell < 20$ ($\ell < 30$ for PolarBear (I)) can only be observed by Planck satellite, we adopt the N^B_ℓ and $f_{\rm sky}$ as the corresponding quantities for Planck satellite. In the scale $\ell = 20$–1000 ($\ell = 30$–1000 for PolarBear (I)), we only adopt the N^B_ℓ and $f_{\rm sky}$ as the corresponding quantities for ground-based experiments.

Case D: In addition to the B-polarization discussed in Case C, we also take into account the observations of the other three power spectra, i.e. $Y = T, C, E$. For $Y = T$ and C, only observed by Planck satellite, we consider the Planck noises and cut sky factor. For $Y = E$, similar with $Y = B$, Planck noise and cut sky factor are considered for $\ell < 20$ ($\ell < 30$ for PolarBear (I)), and the noises and cut sky factors of ground-based experiments are considered for the other multipole scales.

3.1. Best-pivot multipole ℓ^*_t

First, let us discuss PolarBear (II) as a typical ground-based experiment. By solving Eq. (13), in Fig. 2 we plot the best-pivot multipole ℓ^*_t as a function of tensor-to-scalar ratio r in the four cases. In Case A, the value of ℓ^*_t is always smaller than 40, which is because that, in Case A the main contribution on the constraint of RGWs only comes from the observation in the very large scale, i.e. the reionization peak of B-polarization power spectrum [20,25]. In Case B, $50 < \ell^*_t < 130$, the best-pivot multipole is in the intermedial scale, which reflects that PolarBear (II) constrains the RGWs mainly by the observation in the intermedial scale. As a combination of Cases A and B, in Case C the value of ℓ^*_t is focused on the range $40 < \ell^*_t < 90$. If we also consider the other three power spectra, T, E, C in Case D, the value of ℓ^*_t decreases a little when $r > 0.1$, due to the contribution of T, E, C power spectra [25].

In Fig. 3, we also plot the best-pivot multipole ℓ^*_t as a function of r in Case D, where the various ground-based experiments are

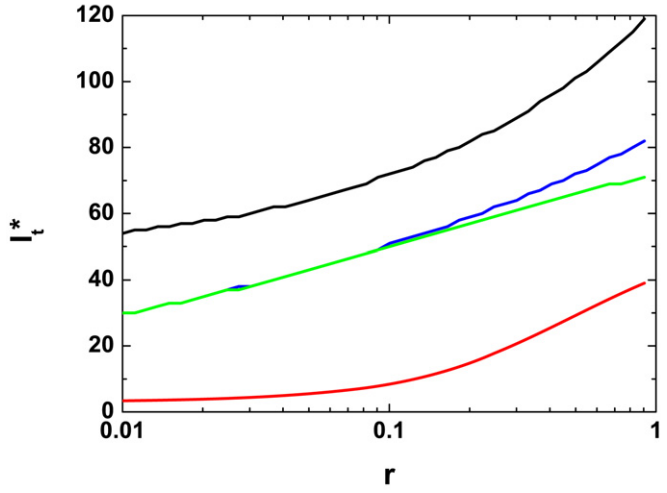

Fig. 2. This figure shows the best-pivot multipole ℓ_t^* for Planck and PolarBear (II) experiments in Case A (red line), Case B (black line), Case C (blue line) and Case D (green line). (For interpretation of the references to colour in this figure legend, the reader is referred to the web version of this Letter.)

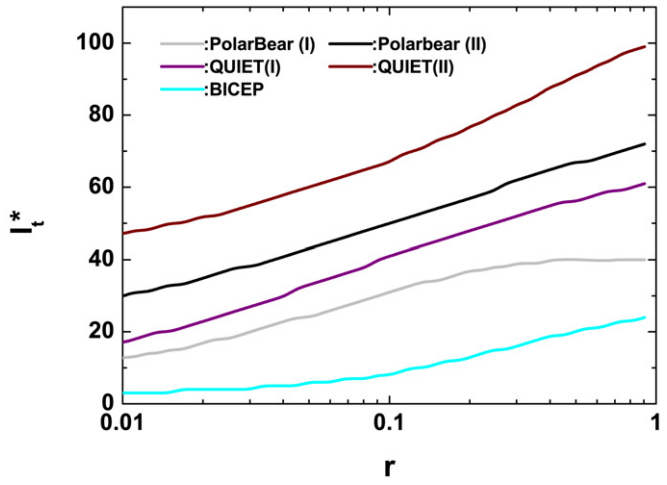

Fig. 3. This figure shows the best-pivot multipole ℓ_t^* in Case D for the various ground-based experiments.

considered. In all these cases, we find that the value of ℓ_t^* increases with the increasing of r. In general, the smaller instrumental noises follow the larger ℓ_t^*.

3.2. Signal-to-noise ratio S/N

Fig. 4 presents the signal-to-noise ratio S/N as a function of r for Planck and PolarBear (II) experiments, which are obtained by using the first formula in Eq. (15). As expected, in all these four cases, a larger r predicts a larger S/N. When $r = 0.1$, $S/N = 3.6$ for Planck satellite, and $S/N = 8.4$ for PolarBear (II) experiment. If we require that $S/N > 3$, $r > 0.07$ must be satisfied for Planck satellite, and $r > 0.02$ for PolarBear (II) experiment. This figure shows that, PolarBear (II) can give a much tighter constraint of r than Planck satellite, due to the much smaller noise level of the PolarBear (II) experiment. Even if we combine Planck and PolarBear (II) experiments, the constraint on r cannot make obvious improvement.

In Fig. 5, we also plot the S/N as a function of r in Case D, where the various ground-based experiments are considered. As expected, the values S/N strongly depend on the instrumental noises and the sky survey factor $f_{\rm sky}$ of the ground-based experiments. The QUIET (II) can very well detect the signal of RGWs (4-σ level), even for the model with $r = 0.01$.

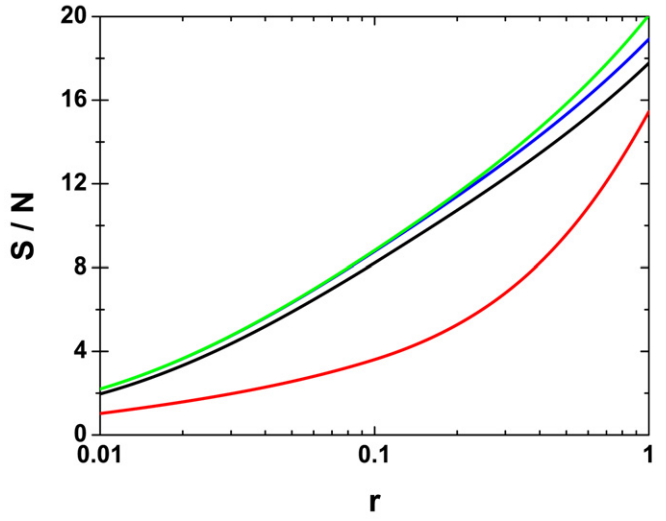

Fig. 4. This figure shows the signal-to-noise ratio S/N for Planck and PolarBear (II) experiments in Case A (red line), Case B (black line), Case C (blue line) and Case D (green line). (For interpretation of the references to colour in this figure legend, the reader is referred to the web version of this Letter.)

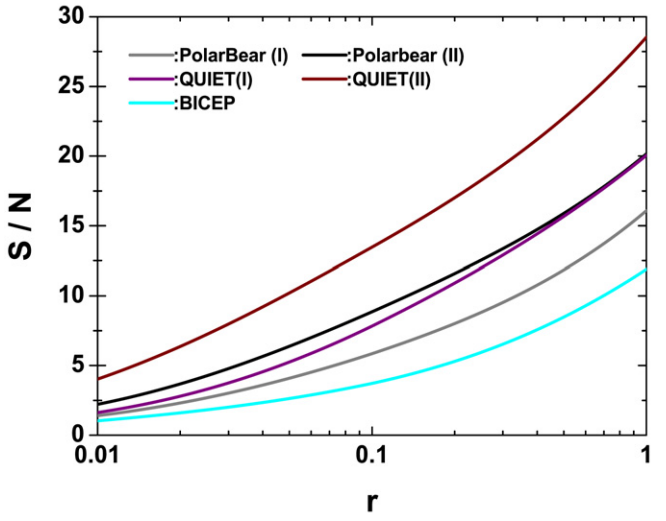

Fig. 5. The figure shows the signal-to-noise ratio S/N in Case D for the various ground-based experiments.

From the first formula in (15), we find the total signal-to-noise ratio can be written as $(S/N)^2 = \sum_\ell (S/N)^2_\ell$, where the individual signal-to-noise ratio for the multipole ℓ is $(S/N)^2_\ell = \sum_Y a^{Y2}_\ell$. Fig. 6 presents the quantity $(S/N)^2_\ell$ as a function of multipole ℓ in the model with parameter $r = 0.1$. This figure clearly shows that, for the Planck satellite the constraint on r mainly comes from the observation in the reionization peak at $\ell < 10$, and for PolarBear (II) experiment, the constraint mainly comes from the observation in the intermedial scale $20 < \ell < 150$. In Cases C and D, the function $(S/N)^2_\ell$ has two peaks, one is at $\ell < 10$, and the other is at $\ell \sim 80$. Comparing with the second peak, the first peak, due to the observation of Planck satellite, is very narrow, and only contribute a fairly small portion for the total S/N. From Fig. 6, we also find the difference between Cases C and D is only at the range $10 < \ell < 20$, due to the observation of the $Y = T, E$ and C power spectra.

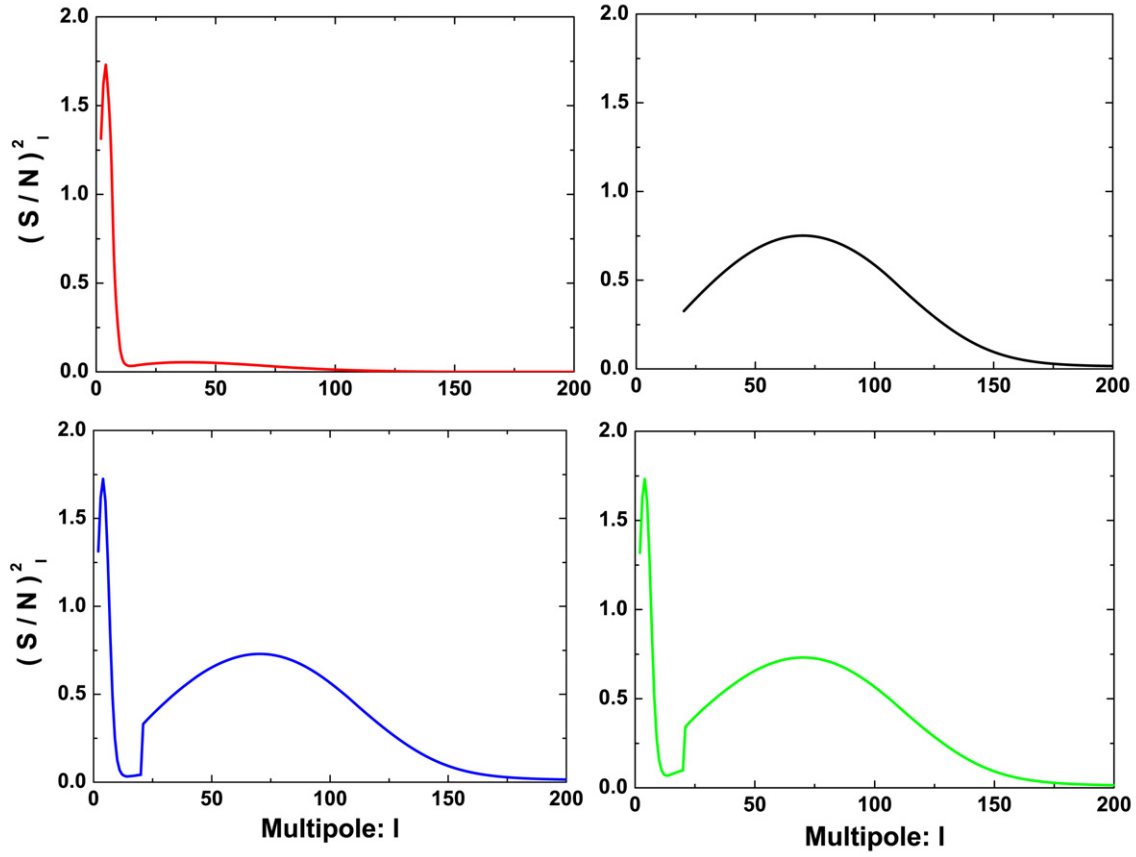

Fig. 6. In the model of $r = 0.1$ for Planck and PolarBear (II) experiment, we plot the individual signal-to-noise ratio $(S/N)^2_\ell$ as a function of multipole ℓ in Case A (red line), Case B (black line), Case C (blue line) and Case D (green line). (For interpretation of the references to colour in this figure legend, the reader is referred to the web version of this Letter.)

3.3. Uncertainty of spectral index Δn_t

Now, let us turn our attention to the constraint of the tensor spectral index n_t. Inserting the best-pivot multipole ℓ_t^* into the second formula in Eq. (15) and taking into account the corresponding noise power spectra, we obtain the Δn_t as a function of r, which are presented in Fig. 7. In this figure, we have considered the Planck and PolarBear (II) experiments. We find that, the value of Δn_t in Case A is similar with that in Case B, although the Planck noise N_ℓ^B is nearly 300 times larger than that of PolarBear (II). When $r > 0.08$, Planck can give a tighter constraint, and when $r < 0.08$, PolarBear (II) can give a tighter constraint. When $r = 0.1$, we find $\Delta n_t = 0.23$ for Case A, and $\Delta n_t = 0.24$ for Case B. Both of them are fairly large for the constraint of the inflationary models. The single-field slow-roll inflationary models predict the consistency relation $n_t = -r/8$ [13], which provides the unique way to exactly test or rule out this kind of models. In order to answer: whether the observations provide the probability to check the consistency relation, we can compare the values of Δn_t with $r/8$. If $\Delta n_t < r/8$, we can say the constraint on n_t is tight enough to check the consistency relation. From Fig. 7, we find that $\Delta n_t < r/8$ is satisfied only if $r > 0.9$ for Case A, and $r > 0.8$ for Case B. Unfortunately, these models have been safely excluded by the current observations [27]. So we conclude that, by either of the single experiment, Planck or PolarBear (II), we cannot constrain n_t tight enough to check the consistency relation.

Now, let us consider Case C, which has combined the Planck and PolarBear (II) experiments. We find in this case, the constraint on n_t becomes much tighter than that in Cases A or B. Comparing with Case B, the value of Δn_t is reduced by a factor 2. When

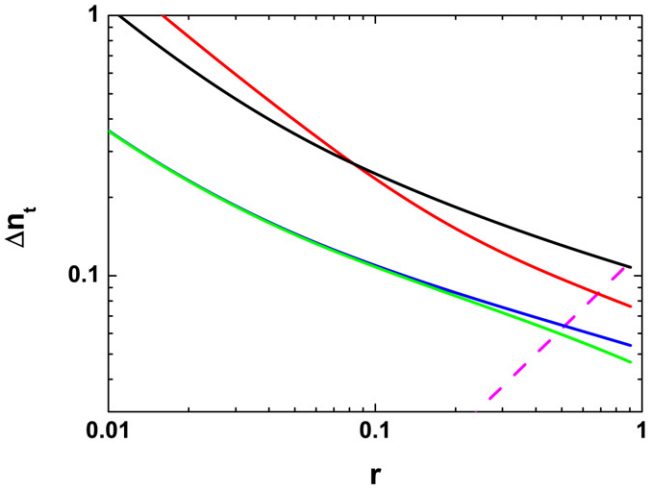

Fig. 7. This figure shows the uncertainty Δn_t for Planck and PolarBear (II) experiments in Case A (red line), Case B (black line), Case C (blue lines) and Case D (green lines). The dashed (magenta) line denote the line with $\Delta n_t = r/8$. (For interpretation of the references to colour in this figure legend, the reader is referred to the web version of this Letter.)

$r = 0.1$, $\Delta n_t = 0.10$, which is much smaller than that in Cases A or B. From Fig. 7, we also find that $\Delta n_t < r/8$ is satisfied only if $r > 0.5$. If considering the contribution of T, E, C, i.e. Case D, the constraint on n_t can be even reduced when $r > 0.2$. So combining the Planck and PolarBear (II) experiments can effectively reduce

the uncertainty of n_t, although the noise power spectra of Planck experiment is much larger than that in PolarBear (II).

In Fig. 8, we also plot the Δn_t as a function of r in Case D, where the various ground-based experiments are considered. We find that, by combing QUIET (II) and Planck experiments, we can get a constraint $\Delta n_t = 0.09$ for the model with $r = 0.1$, and a constraint $\Delta n_t = 0.06$ for the model with $r = 0.3$.

Let us investigate the contribution of the observation in the individual multipole ℓ. From Eq. (15), we find the quantity $(1/\Delta n_t)^2$ is a sum of $\sum_Y (a_\ell^Y b_\ell^*)^2$ for the multipole ℓ. In Fig. 9 we plot the quantity $\sum_Y (a_\ell^Y b_\ell^*)^2$ as a function of ℓ for all the four cases, where we have considered the model with parameter $r = 0.1$. In all cases, the contribution on the constraint of Δn_t mainly comes from the observation in the rage $\ell < 300$. From this figure, we also find that this quantity has the zero value when $\ell = \ell_t^*$, due to $b_\ell^*(\ell = \ell_t^*) = 0$. So the observation around the best-pivot multipole is not important for the constraint of n_t. In the range of $\ell < 300$, when $\ell \ll \ell_t^*$ or $\ell \gg \ell_t^*$, the value of b_ℓ^* is large, as well as the quantity $\sum_Y (a_\ell^Y b_\ell^*)^2$, which gives the important contribute for the constraint of n_t. Especially the observation in the largest scale. For instance, in Case C the best-pivot multipole $\ell_t^* = 51$, so $(b_{\ell=2}^*)^2 = 10.5$ and $(b_{\ell=200}^*)^2 = 1.86$, the former one is 6 times larger than the latter one. So the observation at $\ell = 2$ is much more important than that at $\ell = 200$, for constraining the spectral index n_t. We conclude that, the Planck observation in the largest scale is extremely important for the constraint of n_t, although the noise power spectra of Planck satellite is much larger than that of the ground-based experiments.

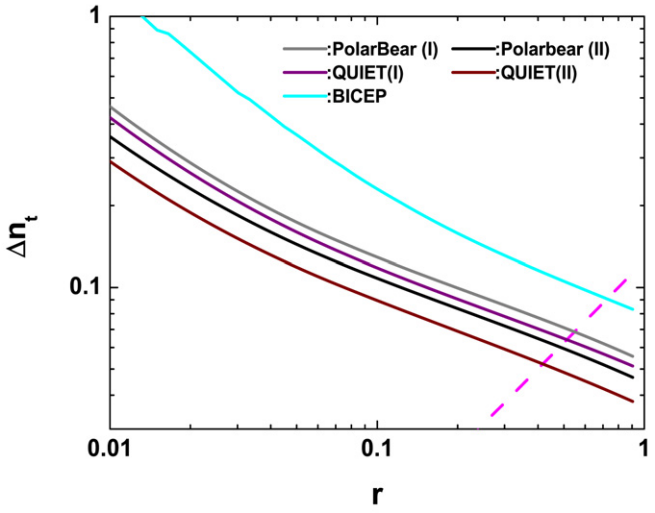

Fig. 8. The figure shows the uncertainty Δn_t in Case D for the various ground-based experiments.

4. Conclusion

Detecting the signal of RGWs is one of the most important tasks for the forthcoming CMB experiments, including the ground-based, space-based and balloon-borne experiments. In this Letter, by calculating the uncertainty of the parameters r and n_t, we compared the detection abilities of the upcoming space-based Planck mission and the various ground-based experiments. Comparing with Planck experiment, ground-based experiments have the much smaller instrumental noise power spectra, but can only observe the CMB field for a small portion of full sky.

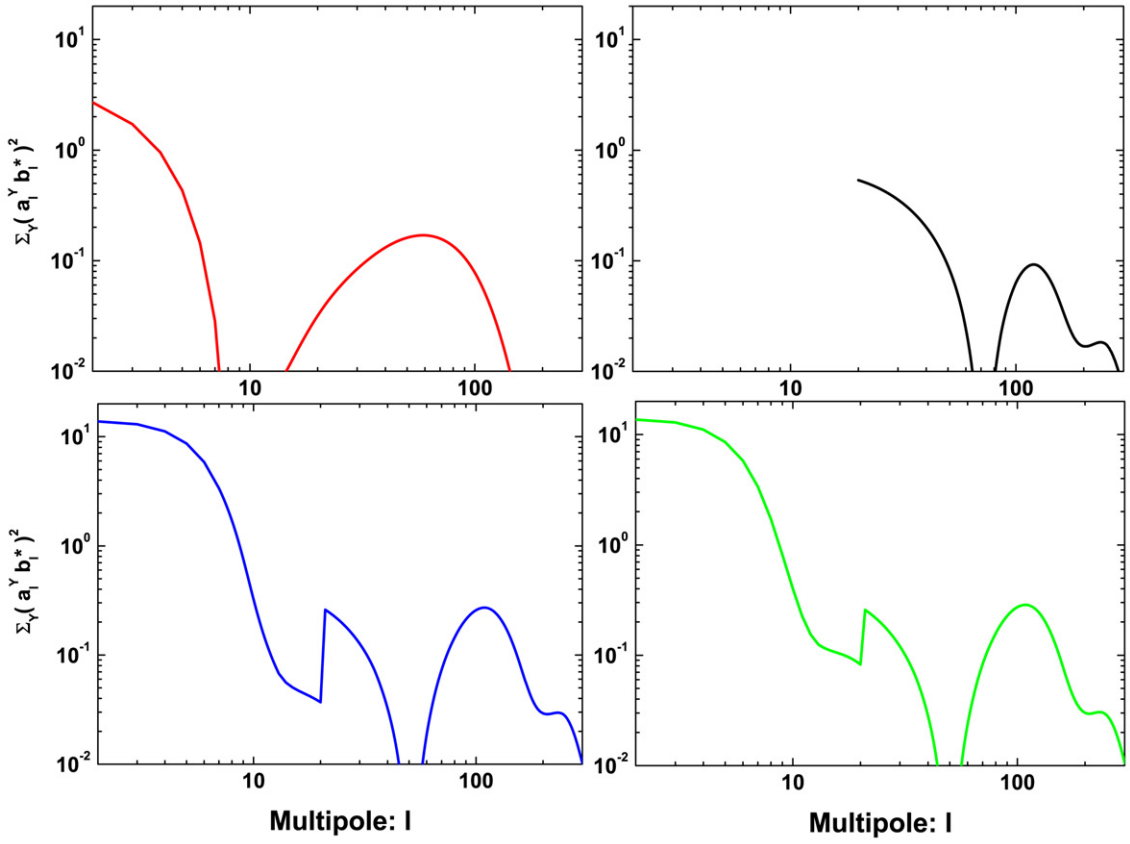

Fig. 9. In the model of $r = 0.1$ for Planck and PolarBear (II) experiments, we plot the quantities of $\sum_Y (a_\ell^Y b_\ell^*)^2$ as a function of multipole ℓ in Case A (red line), Case B (black line), Case C (blue line) and Case D (green line). (For interpretation of the references to colour in this figure legend, the reader is referred to the web version of this Letter.)

Table 2
Instrumental parameters for BICEP experiment [7].

Band center [GHz]	97.7	151.8
N_d	50	48
NET [$\mu K s^{\frac{1}{2}}$]	480	420
FWHM [arcmin]	55	37
f_{sky}	0.024	
ℓ range	20–1000	
Integration time	380 Days	

Table 3
Instrumental parameters for PolarBear (I) experiment [8].

Band center [GHz]	90	150	220
N_d	104	160	96
NET [$\mu K s^{\frac{1}{2}}$]	220	244	453
FWHM [arcmin]	6.7	4.0	2.7
f_{sky}	0.012		
ℓ range	30–1000		
Integration time	0.45 Years		

Table 4
Instrumental parameters for PolarBear (II) experiment [8].

Band center [GHz]	90	150	220
N_d	400	600	200
NET [$\mu K s^{\frac{1}{2}}$]	220	244	453
FWHM [arcmin]	6.7	4.0	2.7
f_{sky}	0.024		
ℓ range	20–1000		
Integration time	0.45 Years		

Table 5
Instrumental parameters for QUIET (I) experiment [9].

Band center [GHz]	40	90
N_d	19	91
NET [$\mu K s^{\frac{1}{2}}$]	160	250
FWHM [arcmin]	23	10
f_{sky}	0.04	
ℓ range	20–1000	
Integration time	2 Years	

Table 6
Instrumental parameters for QUIET (II) experiment [9].

Band center [GHz]	40	90
N_d	1000	1000
NET [$\mu K s^{\frac{1}{2}}$]	160	250
FWHM [arcmin]	23	10
f_{sky}	0.04	
ℓ range	20–1000	
Integration time	3 Years	

We find that ground-based experiments predict a much larger S/N for all the inflationary models, by observing the CMB power spectra in the intermedial multipole range. Even we combine it with Planck experiment, the value of S/N cannot be obviously improved.

By calculating the value of Δn_t, we find ground-based experiments have the similar ability with Planck mission for the determination of n_t. If combining them, the value of Δn_t can be much reduced, which provides an excellent opportunity to distinguish the various inflationary models. We also find that, the observation in the largest scale ($\ell < 20$) is extremely important for determining the spectral index n_t.

Acknowledgements

W. Zhao thanks NAOC and BNU for invitation and hospitality. This work is supported by Chinese NSF under grant Nos. 10703005 and 10775119. In this Letter, we have used the CAMB code for the calculation of CMB power spectra [28].

Appendix A. Instrumental parameters of the various ground-based experiments

In this appendix, we shall list the instrumental parameters for the various ground-based experiment, which including BICEP, PolarBear (I) and (II), QUIET (I) and (II). The parameters are detailed listed in Tables 2–6, separately.

References

[1] L.P. Grishchuk, Zh. Eksp. Teor. Fiz. 67 (1974) 825, Sov. Phys. JETP 40 (1975) 409;
L.P. Grishchuk, Ann. NY Acad. Sci. 302 (1977) 439;
L.P. Grishchuk, Fiz. Pis'ma Zh. Eksp. Teor. 23 (1976) 326;
L.P. Grishchuk, JETP Lett. 23 (1976) 293.
[2] A.A. Starobinsky, JETP Lett. 30 (1979) 682;
V.A. Rubakov, M.V. Sazhin, A.V. Veryashin, Phys. Lett. B 115 (1982) 189;
R. Fabbri, M.D. Pollock, Phys. Lett. B 125 (1983) 445;
L.F. Abbott, M.B. Wise, Nucl. Phys. B 224 (1984) 541;
L.F. Abbott, D.D. Harari, Nucl. Phys. B 264 (1986) 487.
[3] L.P. Grishchuk, Lect. Notes Phys. 562 (2001) 167;
Y. Zhang, Y.F. Yuan, W. Zhao, Y.T. Chen, Class. Quantum Grav. 22 (2005) 1383;
W. Zhao, Y. Zhang, Phys. Rev. D 74 (2006) 043503;
T.L. Smith, H.V. Peiris, A. Cooray, Phys. Rev. D 73 (2006) 123503.
[4] N. Seto, J. Yokoyama, J. Phys. Soc. Jpn. 72 (2003) 3082;
Y. Watanabe, E. Komatsu, Phys. Rev. D 73 (2006) 123515;
W. Zhao, Chin. Phys. 16 (2007) 2894;
K. Nakayama, S. Saito, Y. Suwa, J. Yokoyama, JCAP 0806 (2008) 020;
L.A. Boyle, P.J. Steinhardt, Phys. Rev. D 77 (2008) 063504;
K. Nakayama, S. Saito, Y. Suwa, J. Yokoyama, Phys. Rev. D 77 (2008) 124001;
M. Giovannini, Phys. Lett. B 668 (2008) 44.
[5] C.J. MacTavish, et al., Astrophys. J. 647 (2006) 799;
N. Rajguru, et al., Mon. Not. R. Astron. Soc. 363 (2005) 1125;
CAPMAP Collaboration, Astrophys. J. 684 (2008) 771;
E.M. Leitch, et al., Astrophys. J. 624 (2005) 10;
QUaD Collaboration, Astrophys. J. 692 (2009) 1247;
M.R. Nolta, et al., Astrophys. J. Suppl. 180 (2009) 296.
[6] Planck Collaboration, The science programme of Planck, arXiv:astro-ph/0604069.
[7] K.W. Yoon, et al., astro-ph/0606278.
[8] http://bolo.berkeley.edu/polarbear/index.html.
[9] http://quiet.uchicago.edu/index.php;
D. Samtleben, arXiv:0802.2657.
[10] http://groups.physics.umn.edu/cosmology/ebex/index.html;
http://www.iac.es/project/cmb/quijote/.
[11] A. Kogut, et al., New Astron. Rev. 50 (2006) 1009;
B.P. Crill, et al., arXiv:0807.1548.
[12] B. Keating, P. Timbie, A. Polnarev, J. Steinberger, Astrophys. J. 495 (1998) 580.
[13] D.H. Lyth, A. Riotto, Phys. Rep. 314 (1999) 1.
[14] D. Polarski, A.A. Starobinsky, Phys. Lett. B 356 (1995) 196;
L.P. Grishchuk, Phys. Usp. 48 (2005) 1235, Usp. Fiz. Nauk 175 (2005) 1289;
R.H. Brandenberger, A. Nayeri, S.P. Patil, C. Vafa, Phys. Rev. Lett. 98 (2007) 231302;
J. Grain, A. Barrau, Phys. Rev. Lett. 102 (2009) 081301.
[15] D.N. Spergel, et al., Astrophys. J. Suppl. 170 (2007) 377.
[16] A. Polnarev, Sov. Astron. 29 (1985) 607;
D. Harari, M. Zaldarriaga, Phys. Lett. B 310 (1993) 96;
U. Seljak, M. Zaldarriaga, Phys. Rev. Lett. 78 (1997) 2054;
M. Kamionkowski, A. Kosowsky, A. Stebbins, Phys. Rev. D 55 (1997) 7368.
[17] L.P. Grishchuk, Phys. Rev. D 48 (1993) 5581;
L.P. Grishchuk, Phys. Rev. Lett. 70 (1993) 2371.
[18] M. Zaldarriaga, U. Seljak, Phys. Rev. D 55 (1997) 1830.
[19] J.R. Pritchard, M. Kamionkowski, Ann. Phys. (N.Y.) 318 (2005) 2;
W. Zhao, Y. Zhang, Phys. Rev. D 74 (2006) 083006;
D. Baskaran, L.P. Grishchuk, A. Polnarev, Phys. Rev. D 74 (2006) 083008;
B.G. Keating, A.G. Polnarev, N.J. Miller, D. Baskaran, Int. J. Mod. Phys. A 21 (2006) 2459;
Y. Zhang, W. Zhao, X.Z. Er, H.X. Miao, T.Y. Xia, Int. J. Mod. Phys. D 17 (2008) 1105;
T.Y. Xia, Y. Zhang, Phys. Rev. D 78 (2008) 123005.
[20] W. Zhao, D. Baskaran, L.P. Grishchuk, Phys. Rev. D 79 (2009) 023002.
[21] M.P. Hobson, J. Magueijo, Mon. Not. R. Astron. Soc. 283 (1996) 1133.
[22] M. Bowden, et al., Mon. Not. R. Astron. Soc. 349 (2004) 321.

[23] A. Lewis, A. Challinor, Phys. Rep. 429 (2006) 1.
[24] J. Dunkley, et al., arXiv:0811.3915;
A.A. Fraise, et al., arXiv:0811.3920;
G. Efstathiou, S. Gratton, F. Paci, arXiv:0902.4803.
[25] W. Zhao, Phys. Rev. D 79 (2009) 063003.
[26] W. Zhao, D. Baskaran, Phys. Rev. D 79 (2009) 083003.
[27] E. Komatsu, et al., Astrophys. J. Suppl. 180 (2009) 330.
[28] http://camb.info/.